Simultaneous Identification of Thermophysical Properties of Semitransparent Media Using a Hybrid Model Based on Artificial Neural Network and Evolutionary Algorithm

LIU Yang*, *HU Shaochuang*

Sino-European Institute of Aviation Engineering，Civil Aviation University of China，Tianjin 300300，P. R. China

Abstract: A hybrid identification model based on multilayer artificial neural networks（ANNs）and particle swarm optimization（PSO）algorithm is developed to improve the simultaneous identification efficiency of thermal conductivity and effective absorption coefficient of semitransparent materials. For the direct model，the spherical harmonic method and the finite volume method are used to solve the coupled conduction-radiation heat transfer problem in an absorbing，emitting，and non-scattering 2D axisymmetric gray medium in the background of laser flash method. For the identification part，firstly，the temperature field and the incident radiation field in different positions are chosen as observables. Then，a traditional identification model based on PSO algorithm is established. Finally，multilayer ANNs are built to fit and replace the direct model in the traditional identification model to speed up the identification process. The results show that compared with the traditional identification model，the time cost of the hybrid identification model is reduced by about 1 000 times. Besides，the hybrid identification model remains a high level of accuracy even with measurement errors.

Key words：semitransparent medium；coupled conduction-radiation heat transfer；thermophysical properties；simultaneous identification；multilayer artificial neural networks（ANNs）；evolutionary algorithm；hybrid identification model

CLC number：TK124　　　　**Document code**：A　　　　**Article ID**：1005-1120(2024)04-0458-18

0　Introduction

According to the extent of photon penetration into the medium prior to absorption or scattering, the medium can be categorized as non-transparent, transparent, or semitransparent. Semitransparent materials have been extensively utilized in industrial production and aerospace applications, such as windshields and portholes, ceramic insulation materials in high-temperature furnaces, thermal barrier coatings on high-temperature engine components' surface, and heat insulation tiles on missiles and high-speed spacecraft surface. The rapid and accurate acquisition of thermophysical properties for semitransparent materials (such as thermal conduc-tivity, and absorption coefficient) plays an essential role in material preparation, performance monitoring and performance improvement, which holds significant importance in ensuring the safety and reliability of parts and systems.

The inverse method is a commonly used approach for identifying the thermophysical properties of materials. The fundamental concept of inverse method involves adjusting the value of one or more input parameters of the direct model within a specified range, which aiming to continuously minimize the discrepancy between the output values of the direct model and those of the real system (supposed as known) until reaching a sufficiently small gap. At

this point, the current input parameter value in the direct model can be approximately considered as the value corresponding to that parameter in the real system. Since the parameters to be identified can be derived from the direct model and can be arbitrarily selected, on the premise of measuring the output of the real system, the simultaneous identification of multiple thermophysical parameters of materials under real working conditions can be achieved by solving an optimization problem, with relatively simple operation and lower cost. Moreover, for semitransparent materials, this method can eliminate the influence of thermal radiation and obtain the true thermal conductivity of the material.

According to the principle of inverse method, any inverse problem can be decomposed into two parts: Establishment and resolution of the direct model, as well as parameter identification based on optimal algorithms or others. Taking the thermophysical properties identification problem of semitransparent materials as an example, its direct model involves highly complex nonlinear equations that couple thermal conduction and radiation, making it nearly impossible to obtain a pure analytical solution. Therefore, the numerical simulation has emerged as a crucial approach for studying the internal heat transfer mechanism of such materials. The radiation transfer equation (RTE) in the nonlinear conduction-radiation coupled equations can be solved by using two categories of methods. One category involves tracking the propagation trajectory of photons, such as the ray tracing method[1], the zonal method, the Monte Carlo method, the discrete transfer method[2], etc. These methods offer high solving accuracy and are suitable for dealing with radiation calculation problems involving non-uniformity, anisotropic scattering, complex geometry, variable refractive index, etc. However, due to the fact that radiation is coupled with conduction or convection, although the calculation time of these methods can be reduced under some specific assumptions[3-5], it is still long in general cases. Another category of methods aims to discretize and solve partial differen-

tial equations, such as the finite volume method[6], the finite element method[7], the discrete ordinates method[8], the spherical harmonic function method[9], etc. These methods offer relatively shorter computation time and are suitable for coupled calculations. As for the parameter identification part, the common optimal algorithms include the gradient methods, such as the derivative-based conjugate gradient method, which offers fast computation but may encounter issues such as falling into local optimal solutions. To deal with these challenges, various approaches have been proposed, including adaptive gradient algorithms, the momentum algorithm, the adaptive momentum algorithm[10], etc. Besides, another class of algorithms represented by heuristic algorithms and meta-heuristic algorithms are also applied, such as the liver cancer algorithm (LCA)[11], the parrot optimizer (PO)[12], the slime mould algorithm (SMA)[13], the binary moth search algorithm (BMSA)[14], the hunger games search algorithm (HGSA)[15], the colony predation algorithm (CPA)[16], the weighted mean of vector (INFO)[17], the Harris hawks optimization (HHO)[18], the rime optimization algorithm (RIME)[19], etc. Taking the thermophysical properties identification problem of semitransparent materials as an example, various algorithms have been applied to solve this problem, including the evolutionary algorithm such as the PSO algorithm and its improved versions[20-22], the Lie-group shooting method (LGSM)[23], the improved teaching-learning-based optimization algorithm (ITLBO)[24], and the improved Golden sine algorithm (IGold-SA)[25].

The above studies on algorithm development strategy have improved the accuracy and robustness of the inverse method to a certain extent. However, due to the repeated adjustment of parameters value and brought into the direct model to approach the actual output value during the identification process, for simultaneous identification of multiple parameters of complex direct models, such as the simultaneous identification of thermophysical properties in the multidimensional coupled conduction-radiation

heat transfer model, the inverse method still suffers from relatively long computation time problem. The problem of achieving a balance between accuracy and speed to meet the demand for highly efficient parameter identification in practical engineering problems is a significant issue that requires careful consideration. In order to deal with this problem, several improvement strategies have been proposed. These include a hybrid algorithm that combines the differential evolution algorithm with the stochastic particle swarm optimization (SPSO) algorithm, in which the differential evolution algorithm is used to enhance the best position of individuals during each search[26]. Moreover, an improved social spider optimization algorithm has been suggested[27], as well as employing graphics processing unit (GPU) technology to accelerate the resolution of direct model solved by the Monte Carlo method[28]. In addition, due to its strong self-learning, imitation and prediction ability, artificial neural network (ANN) has shown the potential to replace traditional methods for solving heat transfer problems, and has been increasingly applied to related issues such as the estimation of radiative flux[29] and the identification of boundary conditions[30] in inverse heat conduction problems, the estimation of gas thermo-physical properties[31], as well as the simultaneous identification of particle distribution function and optical constants in inverse thermal radiation problems[32]. Unlike the inverse method which requires repeated adjustment of the value of parameters to be identified and brought into the direct model, the inverse identification speed of the well-trained neural network is nearly instantaneous. However, it should be noted that the effectiveness of learning for an ANN heavily relies on its training data. And it exists a certain gap in terms of robustness when compared to the evolutionary algorithm.

In summary, the current studies on the identification of thermophysical properties of semitransparent materials primarily focus on improving algorithms during the inverse identification process and these methods have reached a relatively mature

stage of development. However, when it comes to simultaneous identification of multiple parameters under the multidimensional coupled conduction-radiation problem, there is still a drawback in terms of long identification time. In this context, various strategies have been suggested to enhance the parameters identification efficiency, including improving the algorithms, utilizing parallel computing technology to accelerate the direct model, as well as employing ANNs to solve the inverse problem. However, as far as author's awareness, there is a scarcity of studies focusing on combining ANNs with evolutionary algorithms to solve the aforementioned problems. Therefore, this paper proposes a hybrid identification model based on ANNs and PSO algorithm for the simultaneous identification of thermal conductivity and effective absorption coefficient of 2D axisymmetric semitransparent media. Within the framework of the inverse method, the ANNs are employed to fit and replace the direct model to accelerate the identification process. Meanwhile, the PSO algorithm is retained for its robustness to accurately achieve the simultaneous identification of thermal conductivity and effective absorption coefficient of semitransparent materials.

1 Direct Model

As shown in Fig.1, the direct model studied is a uniform, isotropic, absorbing, emitting, and non-scattering semitransparent gray cylinder with black body surfaces. The height of the cylinder is H, the radius is R, the environment temperature is T_f, and the convective heat transfer coefficients are h_z and h_r. Since the cylinder satisfies the assumption of axial symmetry, heat transfer only occurs along the height and radius directions. Initially, the cylinder is in thermal equilibrium with the environment. Subsequently, a heat flux $q(r, t)$ is applied to the front surface of the cylinder until $t = t_p$. The convective heat transfer between the cylinder outer surface and the surrounding air is considered while the radiation heat transfer between the cylinder and the environment is neglected.
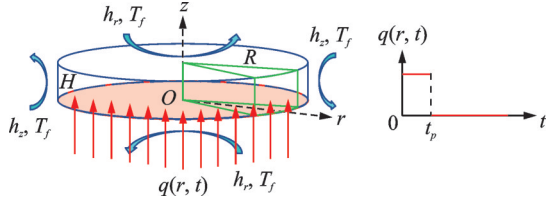
Fig.1 2D axisymmetric direct model and boundary conditions

Considering the coupled conduction-radiation heat transfer mode inside the direct model corresponding to Fig.1, the thermophysical properties to be simultaneously identified are chosen as the thermal conductivity related to the conduction as well as the effective absorption coefficient related to the radiation. The thermal conductivity quantifies the heat conduction capacity of the semitransparent media, while the effective absorption coefficient indicates the degree of photon attenuation inside the 2D axisymmetric model.

The spherical harmonic function method, also known as the P_1 method, is employed to simplify the RTE, which is

$$\nabla\cdot(\nabla G) - 3\kappa^2 G = -12\kappa^2 n^2 \sigma T^4 \qquad (1)$$

where G is the incident radiation, T the temperature, κ the effective absorption coefficient, n the refractive index, and σ the Stefan-Boltzmann constant. The energy equation in the coupled conduction-radiation equations is

$$\frac{\partial T}{\partial t} = \frac{\nabla\cdot(\lambda\nabla T)}{\rho c} + \frac{\dot{q}}{\rho c} =$$

$$\frac{-\nabla\cdot\underbrace{(-\lambda\nabla T)}_{\varphi_c} + \overbrace{\left[-\nabla\cdot\underbrace{\left(-\dfrac{1}{3\kappa}\nabla G\right)}_{\varphi_r}\right]}^{\dot{q}}}{\rho c} \qquad (2)$$

$$\frac{\partial T}{\partial t} = \frac{-\nabla\cdot(\boldsymbol{\varphi}_c + \boldsymbol{\varphi}_r)}{\rho c} = \frac{-\nabla\cdot\boldsymbol{\varphi}_{total}}{\rho c} \qquad (3)$$

where ρ is the density, c the isobaric heat capacity, λ the thermal conductivity, $\dot{q}$ the internal heat source of the medium due to radiation effect, $\boldsymbol{\varphi}_c$ the conduction heat flux, $\boldsymbol{\varphi}_r$ the radiation heat flux under P_1 approximation, and $\boldsymbol{\varphi}_{total}$ the total flux.

Boundary conditions and initial conditions of

the direct model can be written as follows.

For $z = 0$, $\forall(r, t)$, we have

$$\begin{cases} -\lambda\dfrac{\partial T}{\partial z} - \dfrac{1}{3\kappa}\dfrac{\partial G}{\partial z} = \begin{cases} q - h_r(T - T_f) & 0 < t \leqslant t_p \\ -h_r(T - T_f) & t_p < t \end{cases} \\ -\dfrac{2}{3\kappa}\dfrac{\partial G}{\partial z} + G = 4n^2\sigma T^4 \end{cases}$$

$$(4)$$

For $z = H$, $\forall(r, t)$, we have

$$\begin{cases} -\lambda\dfrac{\partial T}{\partial z} - \dfrac{1}{3\kappa}\dfrac{\partial G}{\partial z} = h_r(T - T_f) \\ \dfrac{2}{3\kappa}\dfrac{\partial G}{\partial z} + G = 4n^2\sigma T^4 \end{cases} \qquad (5)$$

For $r = 0$, $\forall(z, t)$, we have

$$\begin{cases} -\lambda\dfrac{\partial T}{\partial r} = 0 \\ -\dfrac{1}{3\kappa}\dfrac{\partial G}{\partial r} = 0 \end{cases} \qquad (6)$$

For $r = R$, $\forall(z, t)$, we have

$$\begin{cases} -\lambda\dfrac{\partial T}{\partial r} - \dfrac{1}{3\kappa}\dfrac{\partial G}{\partial r} = h_z(T - T_f) \\ \dfrac{2}{3\kappa}\dfrac{\partial G}{\partial r} + G = 4n^2\sigma T^4 \end{cases} \qquad (7)$$

For $t = 0$, $\forall(r, z)$, we have

$$T = T_i \qquad (8)$$

$$G = 4n^2\sigma T_i^4 \qquad (9)$$

where T_i is the initial temperature of the cylinder.

The finite volume method is firstly employed to discretize the above coupled equations. Specifically, the second partial derivatives of temperature T and incident radiation G with respect to space are approximated by a second-order central scheme, while the first partial derivative of temperature with respect to time is approximated by a first-order implicit scheme. Subsequently, the tridiagonal systems obtained are iteratively solved by using the Thomas algorithm. The specific approach is as follows: At a given time, the incident radiation field is assumed as known, and the conduction tridiagonal system is firstly solved to obtain the temperature field. Then this obtained temperature field is brought into the radiation tridiagonal system to update the incident radiation field. This process is repeated until convergence is achieved for both temperature and incident radiation fields at that particular moment. Finally,

the validation of the direct model is shown in Fig.2 and Fig.3. In the case of Fig.2, a step thermal excitation is applied on the whole front surface of the cylinder[33], while Fig.3 corresponds to the case where a Dirichlet thermal excitation is applied on the same surface[34]. The relevant parameter settings are shown in Table 1 and Table 2.
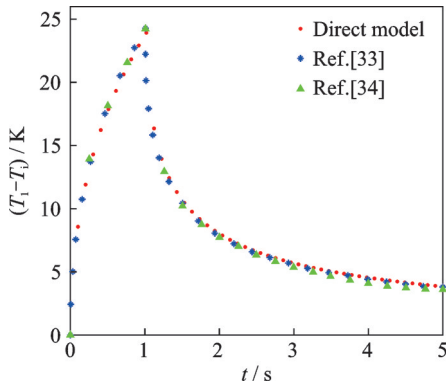

Fig.2 Validation of direct model (step thermal excitation applied on the whole front surface of the cylinder)
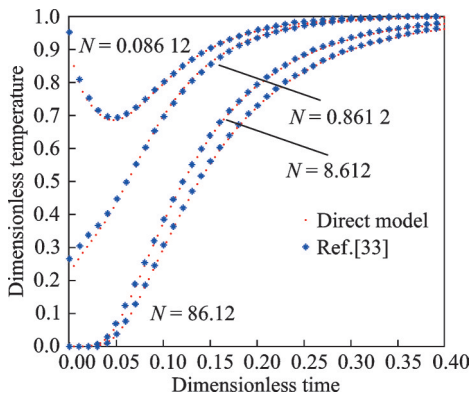

Fig.3 Validation of direct model (Dirichlet thermal excitation applied on the whole front surface of the cylinder)

Table 1 Parameter setting in the case of Fig.2

Parameter	Value
Height H / m	0.01
Radius R / m	0.05
Volumetric heat capacity ρc / (J·m^{-3}·K^{-1})	2.2×10^6
Thermal conductivity λ / (W·m^{-1}·K^{-1})	1.5
Effective absorption coefficient κ / m^{-1}	512
Initial temperature T_i / K	1 000
Refractive index n	1.5
Biot number $Bi_z = h_z H/\lambda$	0
Biot number $Bi_r = h_r R/\lambda$	1.51
Heat flux q / (kW·m^{-2})	50
Heat flux duration t_p / s	1

Table 2 Parameter setting in the case of Fig.3

Parameter	Value
Height H / m	0.01
Radius R / m	0.05
Volumetric heat capacity ρc / (J·m^{-3}·K^{-1})	2.15×10^6
Thermal conductivity λ / (W·m^{-1}·K^{-1})	1
Effective absorption coefficient κ / m^{-1}	10,100,1 000, 10 000
Initial temperature T_i / K	800
Refractive index n	1
Biot number $Bi_z = h_z H/\lambda$	0
Biot number $Bi_r = h_r R/\lambda$	0
Energy density qt_p / (J·m^{-2})	8 600
Energy density duration t_p / s	0.01

The dimensionless time and dimensionless temperature in Fig.3 are respectively defined as $\lambda t/\rho cH^2$ and $(T_1 - T_i)\rho cH/qt_p$, where T_1 is the temperature of front face central point, and N defined as $\lambda\kappa/(4n^2\sigma T_i^3)$ is the conduction-radiation parameter which reflects the relative importance of conduction and radiation in the semitransparent medium. When $N\gg1$, the conduction dominates; when $N\ll1$, the radiation dominates; when $N\approx1$, the conduction and radiation are equally important. The results show that the strategy of using the spherical harmonic method to simplify the RTE and applying the finite volume method to solve the coupled conduction-radiation heat transfer equations has a very good accuracy.

2 Sensibility Study

The sensitivity of observables to parameters is a crucial indicator for assessing the feasibility of parameter identification, which is defined as

$$S = \eta\frac{\partial\Gamma}{\partial\eta} \qquad (10)$$

where Γ and η represent the observables and the parameters to identify. The higher the sensitivity of the observables to the parameters, the easier the identification process will be. Considering that the parameters to be identified are thermal conductivity and effective absorption coefficient, the sensitivity of several observables related to the conduction and

radiation are studied in the case of Table 3. These observables include the temperature of front surface central point T_1, the temperature of cylinder central point T_2, as well as the temperature of rear surface central point T_3 and the incident radiation of rear surface central point G_1.

Table 3   Relevant parameters of the direct model used for the identification process

Parameter	Value
Height H / m	0.002
Radius R / m	0.5
Volumetric heat capacity $\rho c /$ (J·m^{-3}·K^{-1})	1.7×10^6
Initial temperature T_i/ K	1 000
Refractive index n	1.36
Biot number $Bi_z = h_z H/\lambda$	0
Biot number $Bi_r = h_r R/\lambda$	0
Energy density $q t_p /$ (J·m^{-2})	3 399
Energy density duration $t_p/$ s	0.05
Simulation time $t/$ s	2.5

Figs.4—6 show the evolution of sensibility of different observables to λ and κ (left axis), as well as evolution of the ratio of sensibilities (right axis) under different heat transfer modes. The red dotted line and the green solid line respectively represent
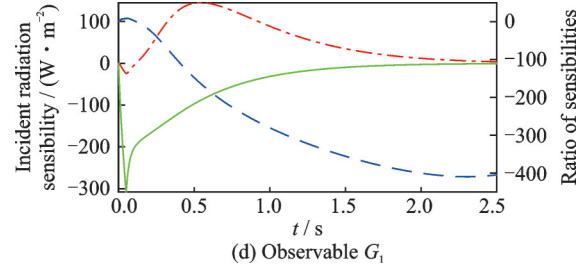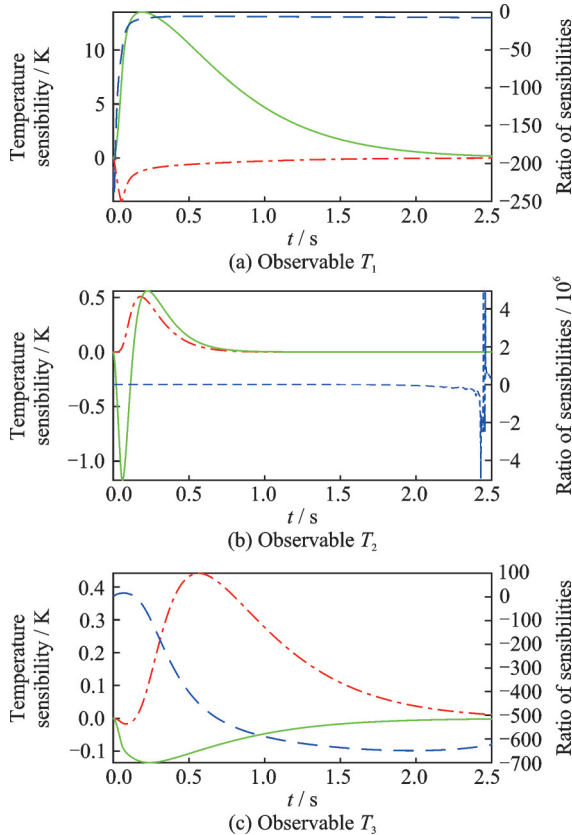

(a) Observable T_1

(b) Observable T_2

(c) Observable T_3

(d) Observable G_1

Fig.4   Evolution of sensibility of different observables to (λ, κ) and evolution of the ratio of sensibilities under the conduction dominant mode ($N = 3.58$)
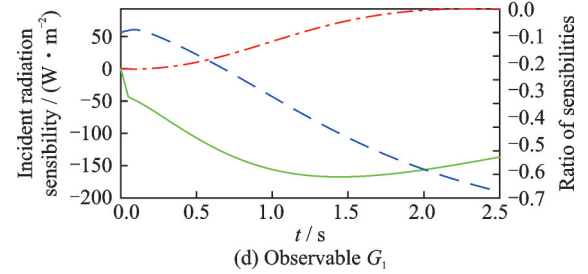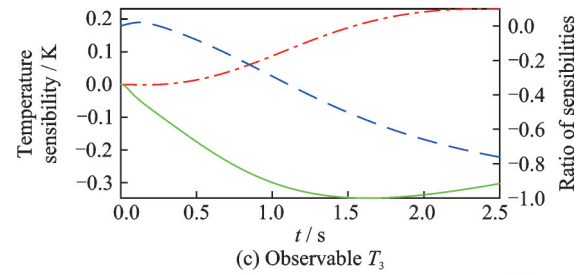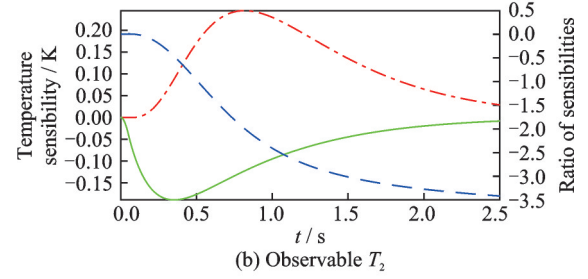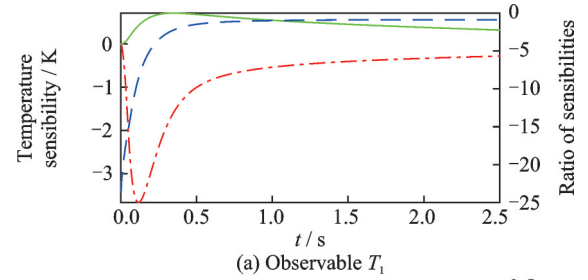

(a) Observable T_1

(b) Observable T_2

(c) Observable T_3

(d) Observable G_1

Fig.5   Evolution of sensibility of different observables to (λ, κ) and evolution of the ratio of sensibilities under the conduction-equivalent mode ($N = 0.95$)

the sensitivity of different observables to λ and κ, while the blue dashed line corresponds to the ratio of the two sensitivities. In Fig.4(a), Fig.4(b), and Fig.6(a), the order of magnitude of the sensitivity curves of observables to κ has been amplified 100
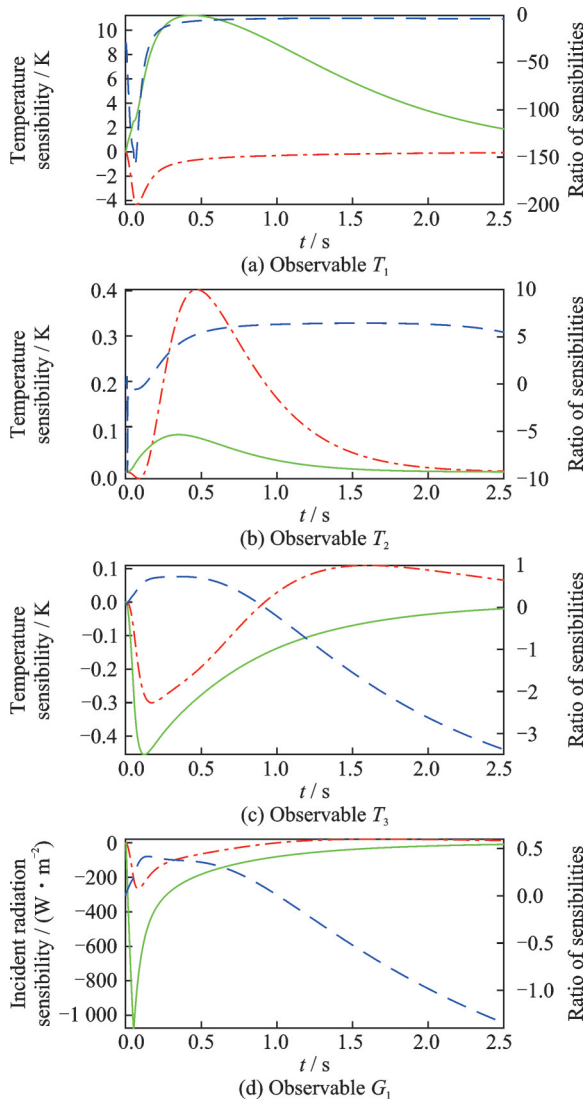
Fig.6   Evolution of sensibility of different observables to (λ, κ) and evolution of the ratio of sensibilities under the radiation dominant mode ($N = 0.48$)

times for ease of viewing. According to these figures, the sensibility of G_1 to κ is almost the highest compared to the other observables. Similarly, the observable with the highest sensitivity to λ is T_1. In

addition, the sensitivities of T_2 and T_3 to λ is in the same order of magnitude, but the sensitivity curves are different from each other. With the transition of the dominant heat transfer mode from radiation to conduction, the sensitivity of G_1 to κ gradually decreases.

3　Hybrid Identification Model

In the framework of inverse method, a hybrid identification model based on multilayer ANNs and PSO algorithm (for simplicity, hereafter referred to as hybrid identification model), is proposed to improve the efficiency of simultaneous identification of multiple thermophysical properties of semitransparent materials. The schematic diagram of the hybrid identification model compared with the traditional identification model based on PSO algorithm (for simplicity, hereafter referred to as traditional identification model), as well as the flowchart of developing the hybrid identification model are respectively illustrated in Fig.7 and Fig.8.

Compared with the traditional identification model with the drawback of long identification time, the hybrid identification model adopts the ANNs to fit the direct model so as to quickly obtain its outputs and speed up the whole identification process. On this basis, instead of using a single complex ANN, four independent neural networks are proposed to reduce the training time cost and training difficulty. More details about the development of the hybrid identification model are presented as follows.
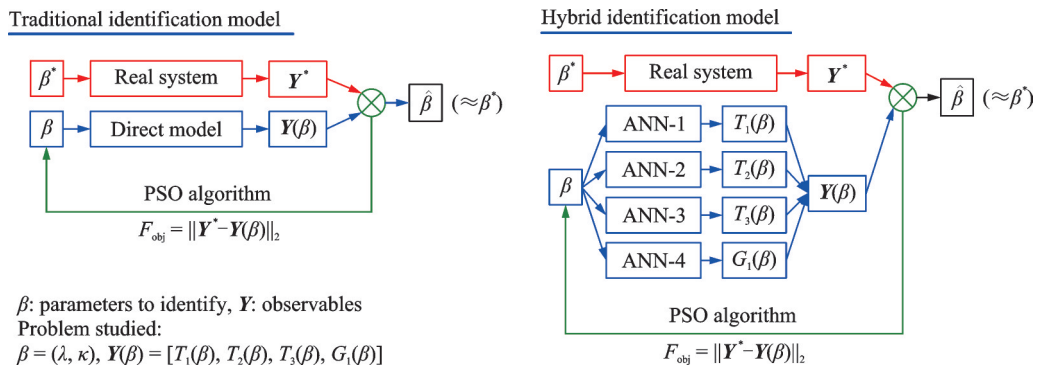

Fig.7   Schematic diagram of the hybrid identification model compared with the traditional identification model
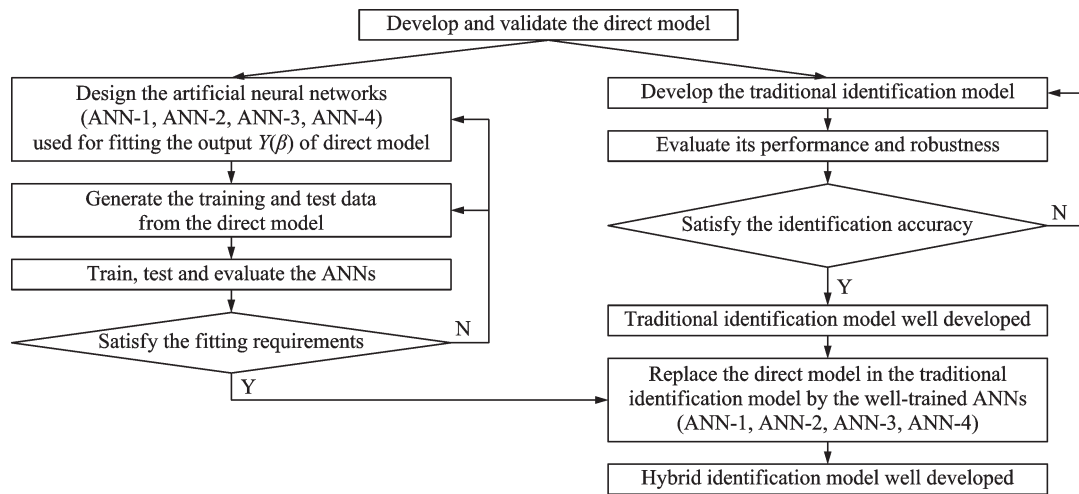
Fig.8   Flowchart of developing the hybrid identification model

First of all, a 2D axisymmetric coupled conduction-radiation heat transfer model, hereinafter referred to as the direct model (DM), is developed and validated. Then, the observables are determined within the framework of the inverse method. According to the sensibility study, the observables include the temperature field at the central point of the front surface, as well as at the central points of both the rear surface and the cylinder. Additionally, the incident radiation field at the central point of the rear surface is also encompassed.

Next, considering that the direct model is relatively complex and more than one parameter are identified at the same time, to accelerate the identification process, four multilayer ANNs with the error back propagation algorithm are used to fit and replace the different outputs of the direct model. The detailed procedure is as follows:

(1) The structure and relevant parameters of the neural networks are firstly determined. Considering that there is more than one observable, four neural networks are built at the same time. The thermal conductivity and effective absorption coefficient to be identified are taken as the inputs of these neural networks, and the four observables, namely the temperature fields at the center point of the front surface and the rear surface, the temperature field at the center point of the cylinder, and the incident radiation field at the center point of the rear surface

are respectively taken as the outputs of the four neural networks. Instead of building a single complex neural network that taking all observables as outputs, the strategy mentioned above builds four independent neural networks. Due to the smaller output dimension of each neural network compared to that of a single complex neural network, the scale of each neural network is smaller (with fewer hidden layers and neurons), which means that the training time for each neural network is shorter. Although there are four neural networks need to be trained, their total training time cost is still much smaller than that of a single complex neural network. In addition, for a single complex neural network, owing to its outputs containing data of different types such as temperature and heat flux, its training is more difficult compared to a neural network with a smaller scale and just one type of observable as output. Considering that four independent neural networks are much faster and easier to train than a single complex neural network, and the purpose of using neural network to fit direct model is just to quickly get accurate outputs (i.e. the four observables above), using four independent neural networks instead of a single complex neural network is a better choice. For each neural network built, there are three hidden layers, each containing 5, 10 and 15 neurons, respectively. The Bayesian regularization function has been chosen as the training algorithm, with a

learning rate of 0.015, a minimum target training error of 10^{-6}, and a maximum number of training iterations set to 10^5. Other relevant parameters of the direct model used for the identification process are shown in Table 3.

(2) 1 500 sets of data containing the parameters to be identified and the corresponding observables information are generated to train these neural networks. These 1 500 sets of training data are evenly divided into three groups based on the different heat transfer mechanisms inside semitransparent materials, which are conduction dominant mode (500 sets), conduction-radiation equivalent mode (500 sets), and radiation dominant mode (500 sets). Taking the case of conduction dominant mode as an example, firstly, the thermal conductivity λ is randomly and uniformly generated in the range of 0.1—5 $W \cdot m^{-1} \cdot K^{-1}$. Secondly, the conduction-radiation parameter N is randomly and uniformly generated in the range of 1.5—50, and the effective absorption coefficient κ corresponding to the above thermal conductivity is derived from the definition of N. Thirdly, each group (λ, κ) generated in the previous step is brought into the direct model and four observables corresponding to the input (λ, κ) are obtained. Finally, each group (λ, κ) and its corresponding observables is combined as one set of training data, and 500 sets of training data under the conduction dominant mode are obtained by following the above three steps. For the cases of conduction-radiation equivalent mode and radiation dominant mode, the generation of 500 sets of training data under each mode following the same steps, except that the range of N varies with the change of dominant mode (conduction-radiation equivalent mode: $N \in [0.5, 1.5]$, radiation dominant mode: $N \in [0.05, 0.5]$).

Compared with generating both λ and κ randomly and uniformly in certain ranges, the training data obtained by the new strategy is more reasonable and consistent with the heat transfer modes within the semitransparent materials, which helps enhancing the efficacy of neural network training.

The mean squared training error for neural networks with temperature as output is the order of magnitudes of 10^{-8}. For the neural network whose output is incident radiation, this error has the order of magnitudes of 10^{-2}. For the above neural networks, the training time cost is generally less than 3 h.

(3) To test the performance of neural networks trained, a series of comparisons are made between the neural networks and the direct model by using 180 sets of test data (60 sets in the case of conduction dominant mode, 60 sets in the case of conduction-radiation equivalent mode, and 60 sets in the case of radiation dominant mode). The results depicted in Figs.9—12 demonstrate that the neural networks exhibit an excellent fitting effect in different heat transfer modes. Specifically, it can be seen from Fig.9 that for each possible heat transfer mode in the semitransparent material, under different combinations of thermal conductivity and effective absorption coefficient, the gap between the temperature of front surface central point obtained by the ANN (icon*) and that obtained by the direct model
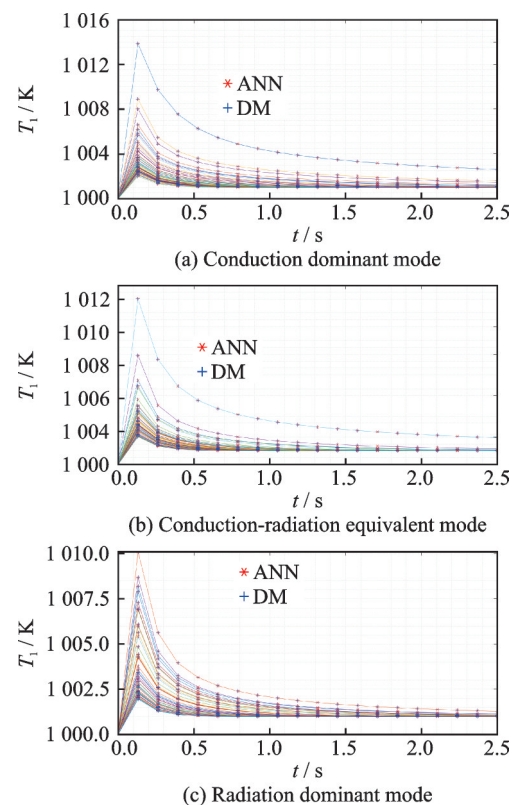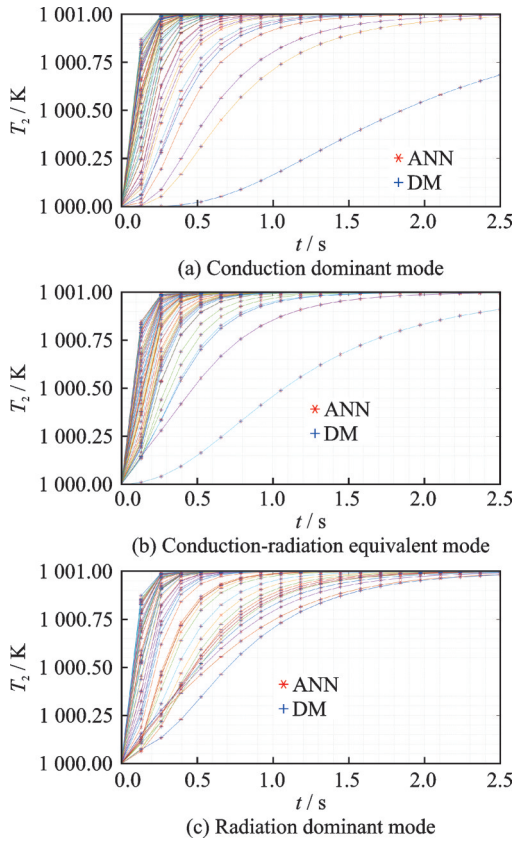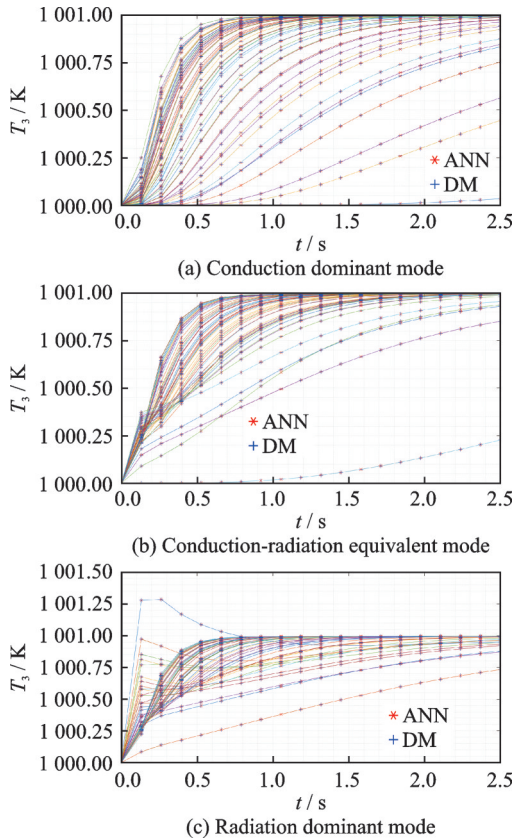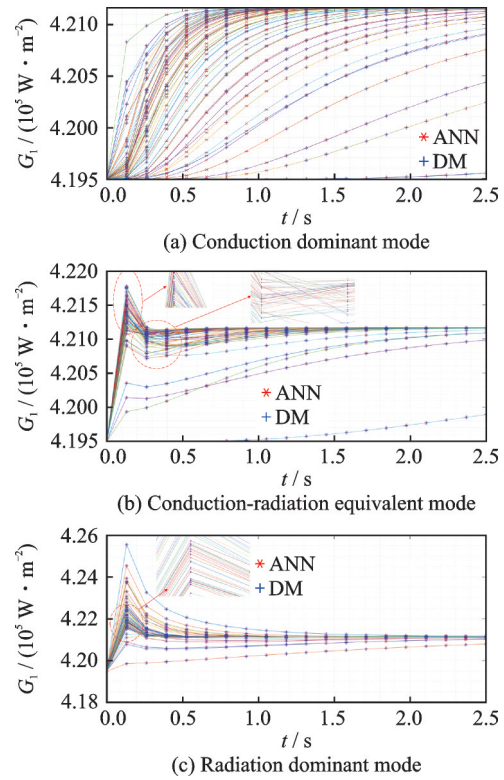

(a) Conduction dominant mode

(b) Conduction-radiation equivalent mode

(c) Radiation dominant mode

Fig.9　Performance test of the ANN (Observable T_1)

Fig.10   Performance test of the ANN (Observable T_2)

Fig.11   Performance test of the ANN (Observable T_3)

Fig.12   Performance test of the ANN (Observable G_1)

(Figs.10—12). After enlarging, although it exists individual cases where the two curves do not completely coincide, the fitting errors of both temperature and incident radiation are all the order of magnitudes of 0.1％. Given that all the possible heat transfer modes in the semitransparent materials as well as the observables related to conduction and radiation are considered and tested, it can be concluded that the neural networks trained can well fit the direct model established in Section 2, which lays a foundation for the subsequent identification part based on the hybrid model.

At last, after replacing the direct model by the well-trained neural networks, the objective function for the identification process is defined as the binomial norms of the difference between the direct model observables (subscript ANN) and real system observables (subscript exp), as shown in Eq.(11). Aiming to reduce the time cost, the value of M, representing the number of discrete temperature and incident radiation values at a specific position varying with time, is significantly smaller ($M=20$) compared to the total number of time nodes N_t.

(icon＋) is small enough, which is the same for other observables under three heat transfer modes

$$F_{\mathrm{obj}} = \sqrt{\sum_{i=1}^{M} \left(T_{1\,\mathrm{ANN}}^i - T_{1\,\mathrm{exp}}^i \right)^2} +$$

$$\sqrt{\sum_{i=1}^{M} \left(T_{2\,\mathrm{ANN}}^i - T_{2\,\mathrm{exp}}^i \right)^2} +$$

$$\sqrt{\sum_{i=1}^{M} \left(T_{3\,\mathrm{ANN}}^i - T_{3\,\mathrm{exp}}^i \right)^2} +$$

$$\sqrt{\sum_{i=1}^{M} \left(G_{1\,\mathrm{ANN}}^i - G_{1\,\mathrm{exp}}^i \right)^2} \qquad (11)$$

For the simultaneous identification of λ and κ, to verify the performance of the hybrid identification model in different cases, three cases are considered, namely the conduction dominant mode, the conduction-radiation equivalent mode and the radiation dominant mode. The target values for each case are respectively set as $(\lambda, \kappa) = (0.5, 400)$, $(0.2, 2\,000)$, $(1.5, 1\,000)$. A PSO algorithm inspired by the cooperation of birds in searching for a target is employed during the inverse identification process. It has a population size of 15 particles, with a maximum iteration number of 50. The search ranges for λ and κ are respectively set to be 0.1—5 $\mathrm{W \cdot m^{-1} \cdot K^{-1}}$ and 100—$5\,000$ $\mathrm{m^{-1}}$, corresponding to a bidimensional search. Eq.(11) is chosen as the objective function and the acceleration coefficients for cognitive learning and social learning are set to 1.49. The above parameters are the main inputs of the PSO algorithm. When the search is finished, for the particle with the global optimal solution, its components in two dimensions are respectively the final identified values of the thermal conductivity and the effective absorption coefficient.
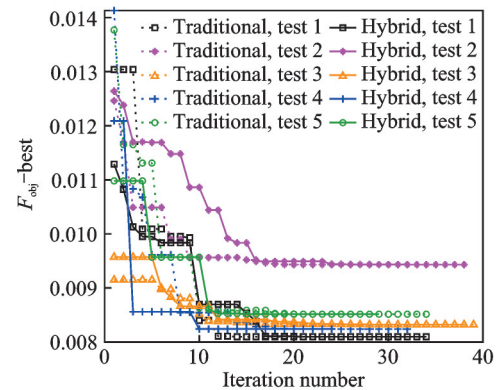
For the fitness curves of PSO algorithm (evolution of global optimal value with iteration number), the results of the first five tests of the hybrid identification model under three heat transfer modes with different noises are presented. The results of the traditional identification model are presented together for the comparison. For simplicity, the word "Traditional" and "Hybrid" are used in the legend to respectively refer to the traditional identification model and hybrid identification model. In fact, these two identification models conducted 690 tests in total, which are too many to all present. The purpose of

presenting the first five tests is just to facilitate the drawing and distinguishment. Although the quantity of tests presented is limited, the overall trend and magnitude of the curves presented here is the same compared to those which are not presented.
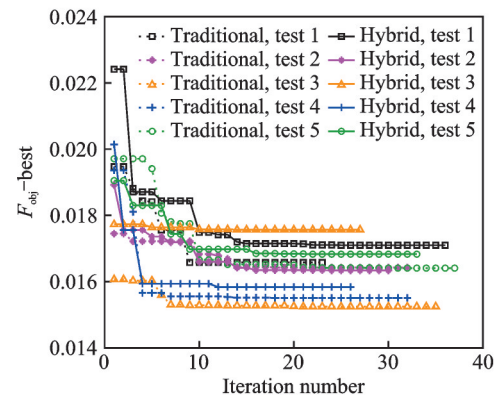
From the fitness curves of PSO algorithm shown in the Figs.13—15, with the increase of random noise, the difficulty of parameter identification and the likelihood of encountering local extreme values under three heat transfer modes gradually in-
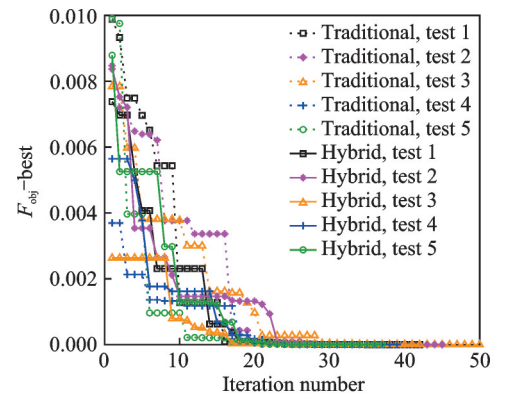
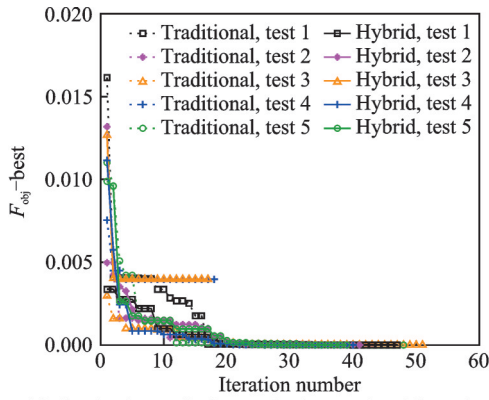(a) Radiation dominant mode with $I_1=0$ and $I_2=0$

(b) Radiation dominant mode with $I_1=1$ and $I_2=1\,500$
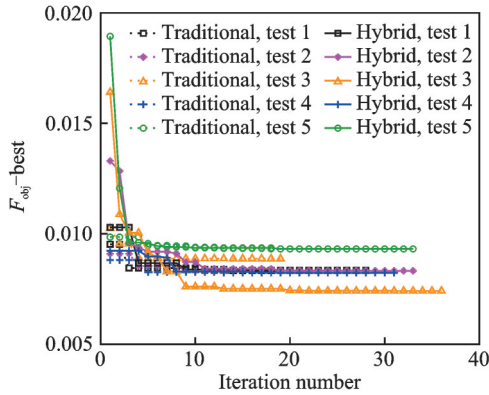
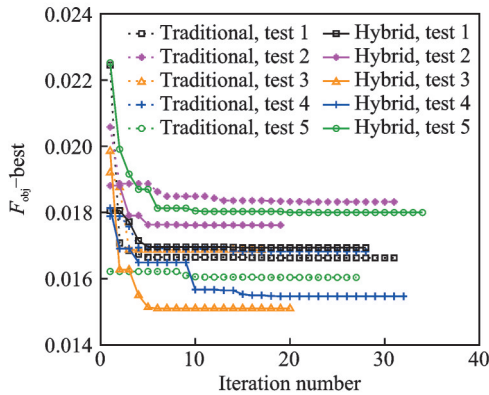(c) Radiation dominant mode with $I_1=2$ and $I_2=3\,000$

Fig.13 Fitness curves of PSO algorithm for the hybrid identification model and traditional identification model under radiation dominant mode and different noise intensities

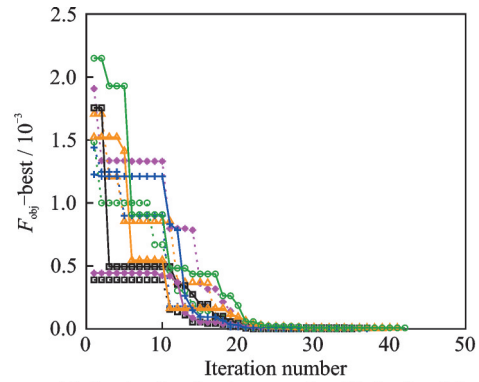(a) Conduction-radiation equivalent mode with $I_1=0$ and $I_2=0$

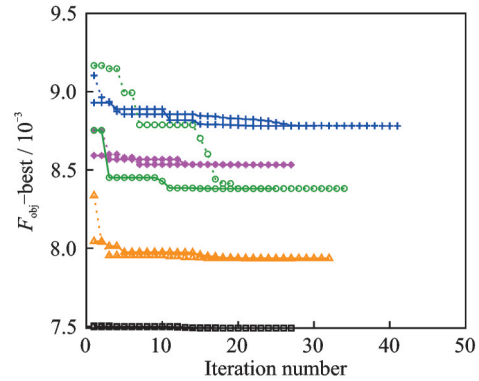(b) Conduction-radiation equivalent mode with $I_1=1$ and $I_2=1\ 500$

(c) Conduction-radiation equivalent mode with $I_1=2$ and $I_2=3\ 000$

Fig.14　Fitness curves of PSO algorithm for the hybrid iden-
tification model and traditional identification model
under conduction-radiation equivalent mode and dif-
ferent noise intensities

(a) Conduction dominant mode with $I_1=0$ and $I_2=0$

(b) Conduction dominant mode with $I_1=1$ and $I_2=1\ 500$

(c) Conduction dominant mode with $I_1=2$ and $I_2=3\ 000$
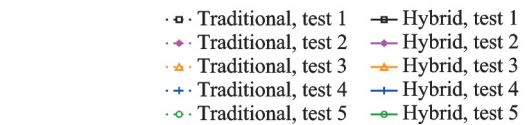
Fig.15　Fitness curves of PSO algorithm for the hybrid iden-
tification model and traditional identification model
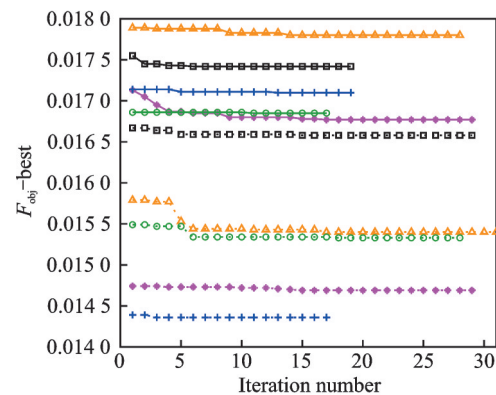under conduction dominant mode and different
noise intensities

crease. This is specifically manifested by the pro-
gressive rise in magnitude of the final global optimal
value achieved by the PSO algorithm, which varies
from 10^{-6} to 10^{-3}, ultimately reaching 10^{-2} under
different noise intensity. Furthermore, when the
search ends, slight difference can be observed in the
global optimal values between the two identification
models due to randomness associated with their ini-
tial positions and speeds within the PSO algorithm.
However, for majority of cases, both identification

models exhibit final global optimal values that are
within a similar order of magnitude, thereby affirm-
ing the robustness and stability of the hybrid model.

　　Moreover, the robustness of the hybrid identifi-
cation model is assessed by adding random noise
$I \times (\text{rand}-0.5)$ to the corresponding observables,
where rand represents a random number ranging

from 0 to 1. Besides, the intensity of noise for temperature and incident radiation is respectively represented by I_1 and I_2 in the following. For each case, the rapidity, the accuracy and the robustness of the hybrid identification model are verified by comparing it with the traditional identification model with the same conditions under different noise intensities, which are $(I_1, I_2)=(0, 0), (1, 1\,500)$ and $(2, 3\,000)$. For these three combinations of noise intensities, 15, 50 and 50 independent identifications are repeated by the hybrid identification model to obtain more general results. Considering that the standard deviation of the parameter identification results may augment with the increase of noise intensity, more repetitions are set for the last two combinations of noise intensity. Tables 4—6 show the comparison results between two kinds of identification models under different heat transfer modes, where the variables $\mu\lambda$ and $\sigma\lambda$ represent the average identification value and standard deviation of λ, while $\mu\kappa$ and $\sigma\kappa$ representing the average identification value and standard deviation of κ. Figs.16—18 represent the distribution of the identified (λ, κ) obtained by the hybrid model with noise added under different cases. Specially, the distribution of identified values of (λ, κ) in different intervals is represented in the form of histograms. The dashed lines represent the Gaussian distribution whose expectation and standard deviation are the average identification value and the standard deviation of the identification results obtained by the hybrid model, which are shown in Tables 4—6.

Table 4   Comparison between two kinds of identification models in the case of radiation dominant

Parameter	$I_1=I_2=0$, 15 identifications		$I_1=1, I_2=1\,500$, 50 identifications		$I_1=2, I_2=3\,000$, 50 identifications	
	Hybrid	Traditional	Hybrid	Traditional	Hybrid	Traditional
$\mu\lambda / (\mathrm{W \cdot m^{-1} \cdot K^{-1}})$	0.499 970	0.500 000	0.499 239	0.499 209	0.504 641	0.510 484
$\sigma\lambda / (\mathrm{W \cdot m^{-1} \cdot K^{-1}})$	1.72E−16	0	0.039 748	0.039 812	0.072 462	0.063 405
$\mu\kappa / \mathrm{m^{-1}}$	400.017 7	400.000 0	392.039 1	392.175 8	409.293 4	420.212 9
$\sigma\kappa / \mathrm{m^{-1}}$	0.001 586	0	55.592 04	55.503 98	154.723 9	133.990 6
Time cost / s	14.01	10 663.06	11.55	9 875.45	11.46	9 172.65

Table 5   Comparison between two kinds of identification models in the case of conduction-radiation equivalent

Parameter	$I_1=I_2=0$, 15 identifications		$I_1=1, I_2=1\,500$, 50 identifications		$I_1=2, I_2=3\,000$, 50 identifications	
	Hybrid	Traditional	Hybrid	Traditional	Hybrid	Traditional
$\mu\lambda / (\mathrm{W \cdot m^{-1} \cdot K^{-1}})$	0.199 961	0.200 000	0.197 438	0.197 445	0.201 788	0.211 537
$\sigma\lambda / (\mathrm{W \cdot m^{-1} \cdot K^{-1}})$	5.16E−06	2.87E−17	0.013 114	0.013 124	0.031 788	0.035 530
$\mu\kappa / \mathrm{m^{-1}}$	1 999.756	2 000.000	2 050.553	2 049.999	2 019.125 9	2 096.968 8
$\sigma\kappa / \mathrm{m^{-1}}$	0.086 293	0.000 106	281.384 8	280.873 0	880.336 8	805.129 7
Time cost / s	13.73	12 385.09	11.00	9 191.70	11.91	8 502.47

Table 6   Comparison between two kinds of identification models in the case of conduction dominant

| Parameter	$I_1=I_2=0$, 15 identifications		$I_1=1, I_2=1\,500$, 50 identifications		$I_1=2, I_2=3\,000$, 50 identifications	
	Hybrid	Traditional	Hybrid	Traditional	Hybrid	Traditional
$\mu\lambda / (\mathrm{W \cdot m^{-1} \cdot K^{-1}})$	1.500 000	1.500 000	1.563 226	1.559 053	1.602 569	1.543 335
$\sigma\lambda / (\mathrm{W \cdot m^{-1} \cdot K^{-1}})$	3.42E−05	0	0.232 583	0.232 616	0.391 109	0.407 742
$\mu\kappa / \mathrm{m^{-1}}$	1 000.213	1 000.000	1 183.213	1 101.468	1 235.623	1 601.092
$\sigma\kappa / \mathrm{m^{-1}}$	0.121 457	9.00E−05	733.459 1	602.101 8	1 319.628	1 521.367
Time cost / s	14.97	11 822.77	9.01	7 900.87	9.59	7 056.97
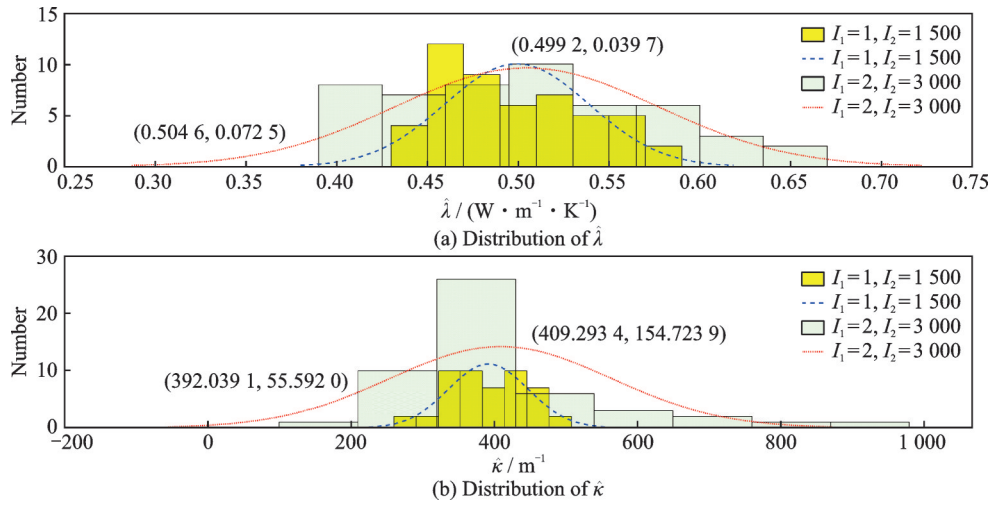
Fig.16   Distribution of identified (λ, κ) obtained by the hybrid model with noise added (Radiation dominant mode)
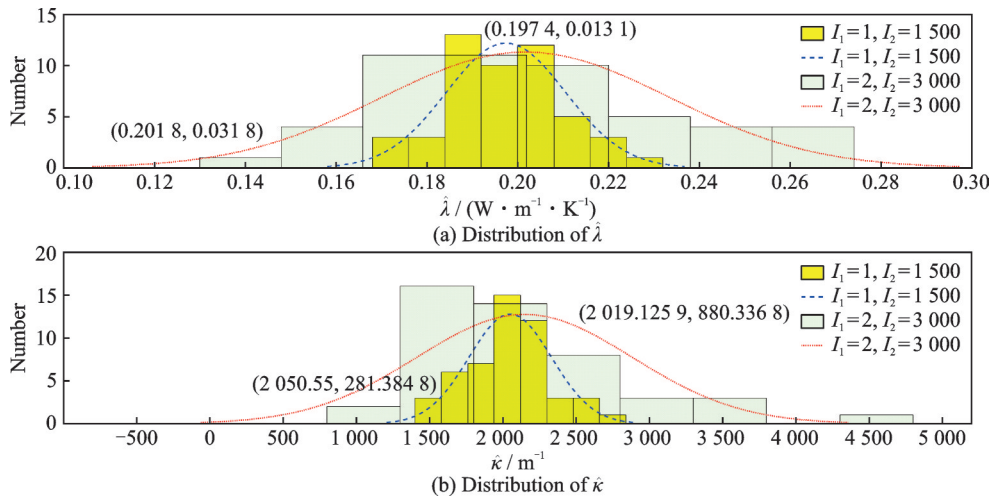

Fig.17   Distribution of identified (λ, κ) obtained by the hybrid model with noise added (Conduction-radiation equivalent mode)
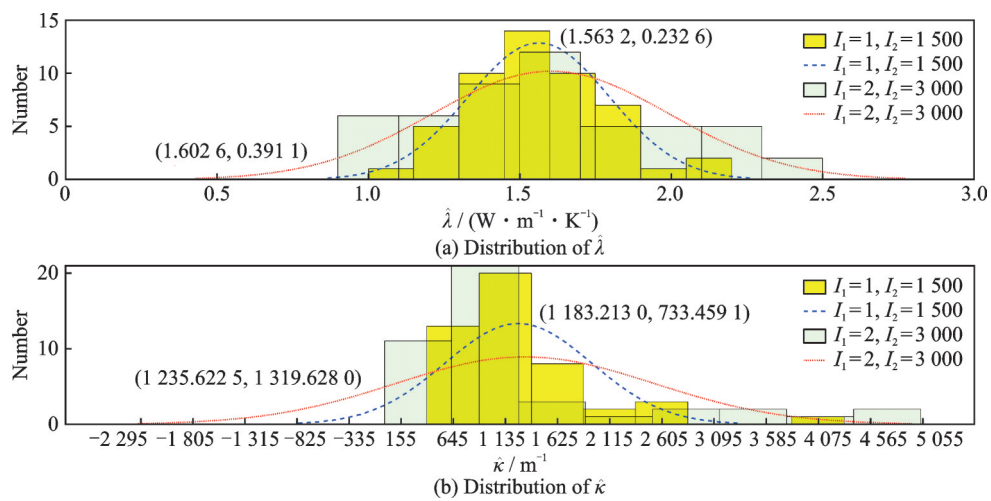
Fig.18   Distribution of identified (λ, κ) obtained by the hybrid model with noise added (Conduction dominant mode)

The above results show that for the simultaneous identification of λ and κ, whether for the conduction dominant mode, conduction-radiation equivalent mode or radiation dominant mode, the hybrid identification model has almost the same average identification values and standard deviations as the traditional identification model. For both two identification models, when there is no noise, the parame-

ters identification accuracy is extremely high. With the augment of noise intensity, the error and standard deviation of the identification results of two models gradually increase and certain identified values appear at the search boundary, which is attributed to inherent limitations of the PSO algorithm. Nevertheless, it is evident that most of identified values are still concentrated around the target value, exhibiting a normal distribution trend overall. Moreover, even facing a relatively large noise intensity, the expected value of this normal distribution aligns closely with the target value, which provides valuable insights for the final evaluation. In all cases, the largest identification errors occur when the conduction dominates, this phenomenon can be explained by the fact that the parameters to be identified have the smallest sensitivities relative to the observables under the conduction dominant mode, which making the identification process more difficult. Finally, with the instantaneous fitting characteristics of neural networks, the time cost of the hybrid identification model has been greatly reduced, from the order of magnitude of 10 000 s to 10 s, which reaches a remarkable improvement of about 1 000 times in speed.

4 Conclusions

A hybrid identification model which combines multilayer ANNs with the PSO algorithm is proposed to enhance the efficiency of simultaneous identification of thermophysical properties of semitransparent materials. For inverse problem, the efficiency of parameter identification can be evaluated by its accuracy and speed. As for the accuracy, taking the simultaneous identification of thermal conductivity and effective absorption coefficient studied in this paper as an example, the dimension of observables is increased by adding incident radiation field information into the objective function, which can effectively improve the identification accuracy of effective absorption coefficient and reduce its standard deviation during the identification process. As for the identifi-

cation speed, to solve the problem of high time cost caused by the increasement of observable dimension and the quantity of simultaneous identification parameters, as well as the complexity of the direct model, a direct model fitting-replacement strategy based on multilayer feedforward ANNs is proposed. The main idea of this strategy is to use the strong learning ability and instantaneous prediction characteristics of neural network to fit and replace the direct model to quickly obtain its output, consequently improve the speed of the whole parameter identification process in a large degree.

The fitting effect of neural network largely depends on the quantity and diversity of the training data used. Although the traditional strategy of randomly generating thermal conductivity and effective absorption coefficient in certain ranges can ensure a uniforme distribution of the above parameters in the training data, it cannot ensure the uniformity of the distribution of different heat transfer modes, which easily causes the problem that the neural network is over-trained in certain heat transfer modes but under-trained in others. Considering that the characteristic of coupled heat transfer mechanism in semitransparent media determines that the priority of the distribution uniformity of heat transfer modes is higher than that of the parameters' distribution uniformity in the training data, a new training data generation strategy based on different heat transfer modes (conduction dominant mode, conduction-radiation equivalent mode, radiation dominant mode) is proposed. The results show that the neural networks based on the new training data generation strategy can deal with the fitting requirements of direct model under different heat transfer modes, with an extremely high fitting accuracy.

Finally, the time cost of the hybrid identification model has been greatly reduced, from the order of magnitude of 10 000 s to 10 s, which reaches a remarkable improvement of about 1 000 times in speed. The robustness of the hybrid identification model is also verified after achieving the objective of

significantly enhancing the identification efficiency. The specific approach involves adding random noise into the observables to simulate the measurement error in the actual process. Since the hybrid identification model retains the PSO algorithm, the identification error of the model is kept in a relatively small range even in the face of relatively large noise. For the future research, the feasibility of applying more kinds of neural networks directly to parameter identification of semitransparent materials or other complex material will be studied, for which the robustness of neural networks will be the focus. In addition, an experimental bench related to the parameter identification will also be developed to study the performance of identification model in real situations.

References

［1］ WEI Linyang, QI Hong, NIU Zhitian, et al. Reverse Monte Carlo coupled with Runge-Kutta ray tracing method for radiative heat transfer in graded-index media[J]. Infrared Physics and Technology, 2019, 99: 5-13.

［2］ DEHGHANIAN A, SARVARI S M H. Transient radiative transfer in variable index media using the discrete transfer method[J]. Journal of Quantitative Spectroscopy and Radiative Transfer, 2020, 255: 107259.

［3］ FAN Chao, LI Xiaolei, XIA Xinlin, et al. An unstructured Monte Carlo ray-tracing method for solving radiative heat transfer in 3D gray semitransparent medium[J]. Journal of Quantitative Spectroscopy and Radiative Transfer, 2019, 225: 110-118.

［4］ FAN Chao, XIA Xinlin, QIU Jian, et al. mcrt-FOAM: A mesh-agglomeration Monte Carlo ray-tracing solver for radiative transfer in gray semitransparent solids[J]. Computer Physics Communications, 2021, 258: 107608.

［5］ SANS M, FARGES O, SCHICK V, et al. Solving transient coupled conductive and radiative transfers in porous media with a Monte Carlo method: Characterization of thermal conductivity of foams using a numerical flash method[J]. International Journal of Thermal Sciences, 2022, 179: 107656.

［6］ ZHANG Biao, XU Chuanlong, WANG Shimin. Generalized source finite volume method for radiative transfer equation in participating media[J]. Journal of Quantitative Spectroscopy and Radiative Transfer, 2017, 189: 189-197.

［7］ WANG Cunhai, FENG Yanyan, YUE Kai, et al. Discontinuous finite element method for combined radiation-conduction heat transfer in participating media[J]. International Communications in Heat and Mass Transfer, 2019, 108: 104287.

［8］ ZHOU Ruirui, LI Benwen. The modified discrete ordinates method for radiative heat transfer in two-dimensional cylindrical medium[J]. International Journal of Heat and Mass Transfer, 2019, 139: 1018-1030.

［9］ GE W J, DAVID C, MODEST M F, et al. Comparison of spherical harmonics method and discrete ordinates method for radiative transfer in a turbulent jet flame[J]. Journal of Quantitative Spectroscopy and Radiative Transfer, 2023, 296: 108459.

［10］ KINGMA D P, BA J. Adam: A method for stochastic optimization[C]//Proceedings of the 3rd International Conference for Learning Representations. San Diego, USA:[s.n.], 2015.

［11］ HOUSSEIN E H, OLIVA D, SAMEE N A, et al. Liver cancer algorithm: A novel bio-inspired optimizer[J]. Computers in Biology and Medicine, 2023, 165: 107389.

［12］ LIAN Junbo, HUI Guohua, MA Ling, et al. Parrot optimizer: Algorithm and applications to medical problems[J]. Computer in Biology and Medicine, 2024, 172: 108064.

［13］ YAO Xianshuang, WANG Huiyu, HUANG Zhanjun. Broad fractional-order echo state network with slime mould algorithm for multivariate time series prediction[J]. Applied Soft Computing, 2024. DOI: org/10.1016/j.asoc.2024.111900.

［14］ FENG Yanhong, WANG Gaige. A binary moth search algorithm based on self-learning for multidimensional knapsack problems[J]. Future Generation Computer Systems, 2022, 126: 48-64.

［15］ LUO Xiaolei, DU Bo, GUI Peng, et al. A hunger games search algorithm with opposition-based learning for solving multimodal medical image registration[J]. Neurocomputing, 2023, 540: 126204.

［16］ TU Jiaze, CHEN Huiling, WANG Mingjing, et al. The colony predation algorithm[J]. Journal of Bionic Engineering, 2021, 18: 674-710.

［17］ AHMADIANFAR I, HEIDARI A A, NOSHAD-

IAN S, et al. INFO: An efficient optimization algorithm based on weighted mean of vectors[J]. Expert Systems with Applications, 2022, 195: 116516.

[18] HEIDARI A A, MIRJALILI S, FARIS H, et al. Harris hawks optimization: Algorithm and applications[J]. Future Generation Computer Systems, 2019, 97: 849-872.

[19] SU Hang, ZHAO Dong, HEIDARI A A, et al. RIME: A physics-based optimization[J]. Neurocomputing, 2023, 532: 183-214.

[20] ZHANG Biao, QI Hong, SUN Shuangcheng, et al. Solving inverse problems of radiative heat transfer and phase change in semitransparent medium by using improved quantum particle swarm optimization[J]. International Journal of Heat and Mass Transfer, 2015, 85: 300-310.

[21] NIU Chunyang, QI Hong, JIA Teng, et al. Research on non-contact measurement algorithm of retrieving the parameters distribution of semi-transparent medium[J]. Journal of Engineering Thermophysics, 2015, 36: 2678-2682. (in Chinese)

[22] FANG Hongyi, JIANG Xinyu, HE Zhenzong, et al. Retrieval of heat radiative property parameters in semitransparent media using improved stochastic particle swarm optimization[J]. Transactions of Nanjing University of Aeronautics and Astronautics, 2023, 40(1): 37-46.

[23] HE Mingjian, QI Hong, ZHANG Wenwen, et al. Estimation of space-dependent thermophysical properties in participating media using a Lie-group shooting method[J]. International Journal of Heat and Mass Transfer, 2018, 127: 1064-1075.

[24] WEI Linyang, QI Hong, LI Guojun, et al. Improved teaching-learning-based optimization for estimation of temperature-dependent radiative properties of semitransparent media[J]. International Journal of Thermal Sciences, 2021, 161: 106694.

[25] ZHANG Pei, SUN Chuang, XIA Xinlin. Improved Gold-SA algorithm for simultaneous estimation of temperature-dependent thermal conductivity and spectral radiative properties of semitransparent medium[J]. International Journal of Heat and Mass Transfer, 2022, 191: 122836.

[26] WEI Linyang, QI Hong, SADAF A I, et al. Simultaneous measurement of space-dependent refractive index and absorption coefficient based on a laser irradiation technique[J]. Measurement Science and Technology, 2018, 29: 104006.

[27] SUN Shuangcheng, QI Hong, REN Yatao, et al. Improved social spider optimization algorithms for solving inverse radiation and coupled radiation-conduction heat transfer problems[J]. International Communications in Heat and Mass Transfer, 2017, 87: 132-146.

[28] MA Chunyang, ZHAO Junming, LIU Linhua, et al. GPU-accelerated inverse identification of radiative properties of particle suspensions in liquid by the Monte Carlo method[J]. Journal of Quantitative Spectroscopy and Radiative Transfer, 2016, 172: 146-159.

[29] ROYER A, FARGES O, BOULET P, et al. A new method for modeling radiative heat transfer based on Bayesian artificial neural networks and Monte Carlo method in participating media[J]. International Journal of Heat and Mass Transfer, 2023, 201: 123610.

[30] WANG Hui, YANG Qingtao, ZHU Xinxin, et al. Inverse estimation of heat flux using linear artificial neural network[J]. International Journal of Thermal Sciences, 2018, 132: 478-485.

[31] SUN Feng, XIE Gongnan, LI Shulei. An artificial-neural-network based prediction of heat transfer behaviors for in-tube supercritical CO_2 flow[J]. Applied Soft Computing, 2021, 102: 107110.

[32] PONCE P, MOLINA A, RODRIGUEZ J. New applications of artificial intelligence [M]. [S.l.]: IntechOpen, 2016.

[33] ANDRE S, DEGIOVANNI A. A new way of solving transient radiative-conductive heat transfer problems[J]. Journal of Heat Transfer, 1998, 120: 943-955.

[34] TAN Heping, MAESTRE B, LALLEMAND M. Transient and steady-state combined heat transfer in semitransparent materials subjected to a pulse or a step irradiation[J]. Journal of Heat Transfer, 1991, 113: 166-173.

Author   Dr. LIU Yang received his Ph.D. degree in energy, heat and combustion from Ecole Nationale Supérieure de Mécanique et d'Aérotechnique, Poitiers, France in 2020. He currently works in Civil Aviation University of China.

His research is focused on heat transfer, inverse problems and relevant fields.

Author contributions　Dr. LIU Yang developed the model，wrote the manuscript and completed the revision of the manuscript. Mr. **HU Shaochuang** participated in the discussion，completed part of the calculation work and the revision of the manuscript. All authors commented on the manuscript draft and approved the submission.

Competing interests　The authors declare no competing interests.

（Production Editor：SUN Jing）

基于人工神经网络与演化算法混合模型的半透明介质热物性同时反演

刘　洋，胡少闯

（中国民航大学中欧航空工程师学院，天津 300300，中国）

摘要：为了提高对半透明材料导热系数和等效吸收系数的同时反演效率，本文提出了一种基于多层人工神经网络（Artificial neural networks，ANNs）和粒子群优化（Particle swarm optimization，PSO）算法的混合反演模型。对于正向模型，在激光闪光法的背景下，采用球谐法和有限体积法求解了吸收、发射、非散射的二维轴对称灰介质中的导热-辐射耦合传热问题。对于反演部分，首先选取不同位置的温度场和入射辐射场作为观测量，随后建立了基于PSO算法的传统反演模型，最后构建了ANNs来拟合并替代传统反演模型中的正向模型，以达到加快反演速度的目的。结果表明，与传统反演模型相比，混合反演模型的时间成本降低约1 000倍。此外，即使在有测量误差的情况下，混合模型依旧保持了较高的精度。

关键词：半透明介质；导热-辐射耦合传热；热物性；同时反演；多层人工神经网络；演化算法；混合反演模型